

Tetragonal Nanophase Stabilization in Nondoped Sol–Gel Zirconia Prepared with Different Hydrolysis Catalysts

X. Bokhimi,^{*,1} A. Morales,^{*} O. Novaro,^{*,2} M. Portilla,[†] T. López,[‡] F. Tzompantzi,[‡] and R. Gómez[‡]

^{*}Institute of Physics, The National University of Mexico (UNAM), A.P. 20-364, 01000 México, D.F., Mexico; [†]Faculty of Chemistry, The National University of Mexico (UNAM), A.P. 70-197, 01000 México, D.F., Mexico; [‡]Department of Chemistry, Universidad Autónoma Metropolitana, A.P. 55-534, 09349 México, Mexico

Received March 6, 1997; accepted June 16, 1997

Sol–gel zirconia was prepared with zirconium *n*-butoxide and HCl, H₂SO₄, C₂H₄O₂, and NH₄OH as hydrolysis catalysts. Samples were characterized with DTA and TG analysis, X-ray powder diffraction, and FTIR spectroscopy. The structure of the crystalline phases was refined by the Rietveld method. When samples were annealed below 300°C, they lost weight and had an amorphous structure that, by annealing at higher temperatures, crystallized into nanostructures. For H₂SO₄ as hydrolysis catalyst, the amorphous structure was stable even at higher temperatures, which was probably caused by the presence of SO_x ions in the structure. The local order in the amorphous phase was similar to the local order in the tetragonal zirconia. Crystallization of the amorphous phase produced tetragonal and monoclinic nanophases, with the tetragonal as the main phase. Both phases had a similar average crystallite size. By annealing, the tetragonal nanophase, which was more stable when C₂H₄O₂ was the hydrolysis catalyst, was transformed into the monoclinic nanophase. Since not only OH[−] ions in the structure were detected with FTIR spectroscopy but also Zr vacancies were measured with X-ray powder diffraction in the zirconia crystalline structure, we propose that these defects stabilized the tetragonal phase. Both defects disappeared when samples were annealed at high temperatures, which brought about the irreversible transformation of the tetragonal into the monoclinic structure. © 1998

Academic Press

1. INTRODUCTION

The interesting structural and electronic properties of zirconia (ZrO₂) have been put to use in many applications. Since it has a high melting point and low thermal conductivity at high temperature, zirconia is used as a thermal shield (1). In zirconia composites, the martensitic transformation from tetragonal to monoclinic zirconia produces materials with high toughness (2). When zirconia is doped with

divalent or trivalent cations, its structure is deficient in oxygen, which favors oxygen transportation and produces ionic conduction. Therefore, zirconia can be used as an oxygen sensor (3) and in the fabrication of fuel cells (4). These mechanical and electronic properties were discovered and studied mainly in microcrystalline zirconia (5), but recently they have also been studied in nanocrystalline zirconia.

During the past 10 years, nanocrystalline zirconia has been produced by using different methods (6–10). The small size of these crystals favors zirconia sintering at low temperatures (7), the preparation of zirconia thin films (8), and their use as a support in catalysis (11).

In contrast to microcrystalline pure zirconia, where the phase at room temperature is monoclinic, in nanocrystalline pure zirconia, the phase at this temperature can be tetragonal or monoclinic, depending on the preparation conditions (12–15). In microcrystalline zirconia, the stabilization of the tetragonal zirconia phase at room temperature is done by doping it with a large ion such as Y, Ce, Mg, or Ca (5). By annealing, this stabilized tetragonal phase is reversibly transformed into monoclinic zirconia through a martensitic transformation (5).

The initial crystalline phase obtained in nanocrystalline nondoped zirconia depends on the preparation conditions (6, 9, 16). It can be tetragonal or monoclinic. When nanocrystalline nondoped zirconia is annealed, the tetragonal phase is transformed into the monoclinic phase (12). This transformation, however, is neither martensitic nor reversible (17). In this case, some research groups suggest that the transformation is associated with the growth of the tetragonal crystallite size (12), like the dependence of the tetragonal to monoclinic transformation observed in polycrystalline zirconia (18).

One method for making nanocrystalline zirconia is the sol–gel technique, where the final product depends on many parameters (6). Among them, the hydrolysis catalyst and temperature play important roles, especially when multiple nanocrystalline phases coexist in the system (19).

¹ To whom correspondence should be addressed.

² Member of El Colegio Nacional, Mexico.

In the particular case of nanocrystalline zirconia, the formation of the tetragonal or monoclinic nanophase in the initial step of crystallization depends on pH, which in the sol-gel technique can be controlled with the hydrolysis catalyst.

The concentration of the nanophases in the samples and their crystallography can be obtained from X-ray powder diffraction and refinement of their crystalline structure (19). Therefore, in the present work, we have used these techniques for studying the nanophases in the sol-gel zirconia prepared with different hydrolysis catalysts and annealed in air at different temperatures.

2. EXPERIMENTAL

Sample Preparation

With continuous stirring, 10 ml of zirconium *n*-butoxide was dissolved in 150 ml of *tert*-butyl alcohol, and the mixture was refluxed at 70°C. The corresponding hydrolysis catalyst, HCl or H₂SO₄ for pH 3, C₂H₄O₂ for pH 5, and NH₄OH for pH 9, was added until the desired pH was obtained. Then the solution was stirred and refluxed for 10 min and cooled to 50°C. At this temperature, 25.66 ml of water was added dropwise to the solution. Then its temperature was again raised to 70°C, and the solution was stirred and refluxed until forming a gel, which was dried in air at 100°C for 24 h (fresh sample).

Before the analysis, fresh samples were annealed in air at 200, 400, 600, and 800°C for 12 h at each temperature.

DTA and TG Analysis

These analyses were done in a Dupont Model 950 thermoanalyzer with DTA and TGA stages. Samples were annealed in air from 25 to 1200°C at the annealing rate of 20°C/min.

X-Ray Diffraction

The crystalline structure of the phases in the samples was characterized by X-ray powder diffraction and by refining it by the Rietveld method. X-ray diffraction patterns were measured at room temperature with a Siemens D-5000 diffractometer having CuK α radiation and a secondary-beam graphite monochromator. Specimens were prepared by packing sample powder into a glass holder. Intensity was measured by step scanning in the 2θ range between 20° and 110°, with a step of 0.02° and a measuring time of 2 s per point. Crystalline structures were refined by using the DBWS-9411 (20) and WYRET (21) programs. The peak profiles, modeled with a pseudo-Voigt function, had average crystallite size and microstrain as profile-breadth fitting parameters (22). The standard deviations, showing the variation of the last figures of the corresponding number, are

given in parentheses. When the numbers corresponded to parameters obtained from the Rietveld refinement, the estimated standard deviations are not estimates of the analysis as a whole but only of the minimum possible probable errors based on their normal distribution (23).

FTIR Spectroscopy

Transparent disks, obtained by pressing dried sample powder, were characterized with a 170-SX Nicolet FTIR spectrometer.

3. RESULTS AND DISCUSSION

Sol-gel zirconia samples lost weight when they were annealed from room temperature to 300°C (Fig. 1). This weight loss was produced by evaporation of the residual volatile components involved in sample preparation. Above this temperature, the sample weight loss depended on the hydrolysis catalyst.

For all hydrolysis catalysts, the structure of the samples annealed below 300°C was amorphous (Fig. 2A). The center of the main broad peak of the amorphous phase, however, corresponded to the position of the main peak associated with the (011) reflection of the tetragonal zirconia (Fig. 2B). This broad peak was produced by the most frequent ion-ion distances in the amorphous structure, which, in the present case, corresponded to Zr-O distances. This means that the local order in the amorphous phase was similar to the local order in the tetragonal zirconia phase. This explains why the most abundant crystalline phase formed during the crystallization of the amorphous phase was the tetragonal one.

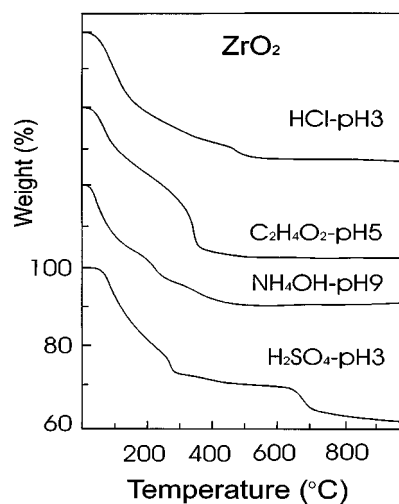


FIG. 1. TG curves as a function of temperature of the sol-gel zirconia prepared with different hydrolysis catalysts.

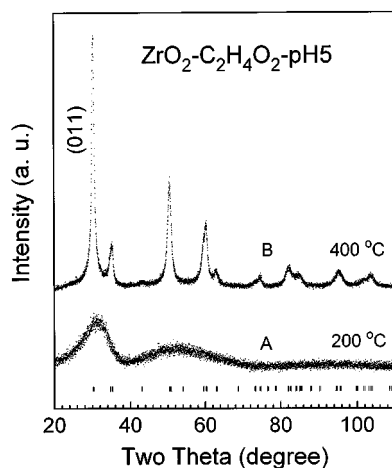


FIG. 2. X-ray diffraction patterns of the sol-gel zirconia prepared with acetic acid as hydrolysis catalyst and annealed in air: (A) at 200°C; (B) at 400°C. The tick marks and the (011) reflection represent the tetragonal zirconia.

When HCl, $C_2H_4O_2$, and NH_4OH were the hydrolysis catalysts, the amorphous structure crystallized when samples were annealed in air at 400°C (Figs. 3–5). During the annealing from room temperature to 400°C, samples lost between 30 and 34% of their initial weight (Fig. 1). Their differential thermal analysis showed that crystallization of the amorphous phase for these hydrolysis catalysts occurred between 300 and 350°C; the precise crystallization temperature depended on the specific hydrolysis catalyst.

When H_2SO_4 was the hydrolysis catalyst, samples crystallized at temperatures higher than 400°C (Fig. 6). Here, the sample annealed until 400°C lost only 26% of its initial

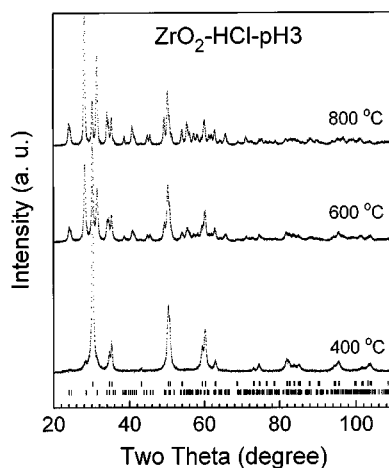


FIG. 3. X-ray diffraction patterns of the sol-gel zirconia prepared with hydrochloric acid as hydrolysis catalyst. Upper tick marks represent the tetragonal zirconia, while lower tick marks represent the monoclinic zirconia.

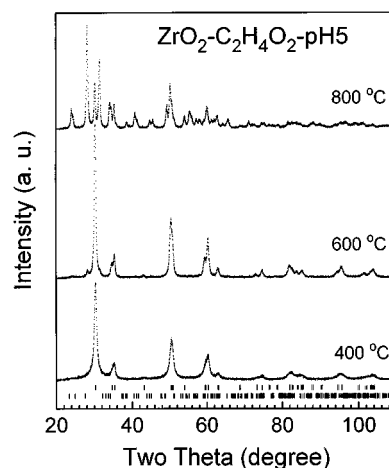


FIG. 4. X-ray diffraction patterns of the sol-gel zirconia prepared with acetic acid as hydrolysis catalyst. Upper tick marks represent the tetragonal zirconia, while lower tick marks represent the monoclinic zirconia.

weight, and annealing at temperatures above 600°C caused additional weight loss (Fig. 1), totaling 37% at 800°C. This weight loss was similar to the total weight loss found in the samples prepared with the other hydrolysis catalysts. This means that the interaction of SO_x ions with the amorphous phase stabilized its amorphous structure and shifted its crystallization to higher temperatures. This was confirmed by the corresponding differential thermal analysis and the weight loss observed above 600°C (Fig. 1). This result will be of interest to those research groups studying zirconia superacids (24–27).

For all hydrolysis catalysts, crystallized samples had two nanocrystalline phases, whose structures were refined by the

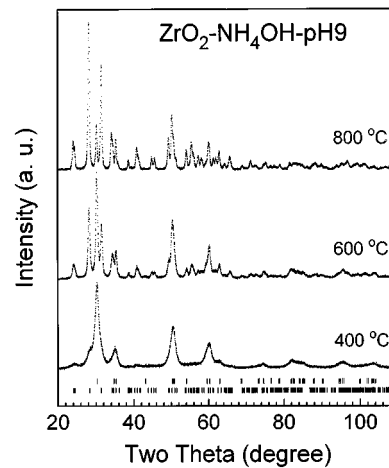


FIG. 5. X-ray diffraction patterns of the sol-gel zirconia prepared with ammonium hydroxide as hydrolysis catalyst. Upper tick marks represent the tetragonal zirconia, while lower tick marks represent the monoclinic zirconia.

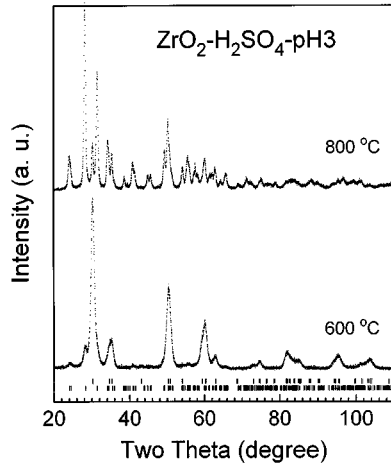


FIG. 6. X-ray diffraction patterns of the sol-gel zirconia prepared with sulfuric acid as hydrolysis catalyst. Upper tick marks represent the tetragonal zirconia, while lower tick marks represent the monoclinic zirconia.

Rietveld method (Figs. 7–10). One crystalline nanophase was tetragonal, described by space group $P4_2/nmc$ and the atom positions given in Table 1. The other nanophase was monoclinic, described by space group $P2_1/c$ and the atom positions given in Tables 2 and 3. These nanostructured phases had crystallite sizes that varied between 4 and 34 nm (Table 4). When acetic acid was the hydrolysis catalyst, the sample annealed at 400°C was composed of 62(3) wt% of the crystalline tetragonal zirconia phase and 38(1) wt% of an amorphous phase with the same local order as the crystalline tetragonal phase (Fig. 8). This amorphous

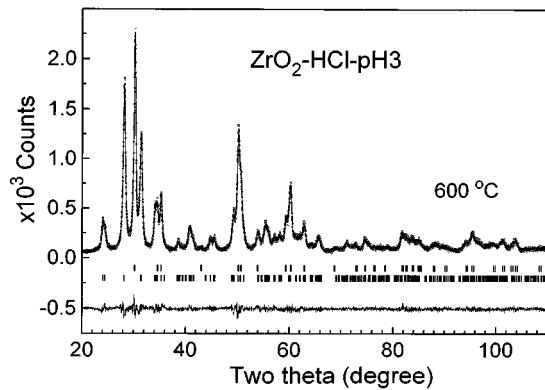


FIG. 7. Rietveld refinement plot of the sol-gel zirconia prepared with hydrochloric acid and annealed in air at 600°C. Experimental data are indicated by dots, while the calculated curve obtained after the refinement is indicated with a continuous line. The residue R_{wp} generated when all contributing parts were taken into account was 0.08. The residue R_F associated with only one phase was 0.009 for the tetragonal zirconia and 0.01 for the monoclinic zirconia. The continuous curve under the tick marks in the difference between the experimental data and the calculated curve.

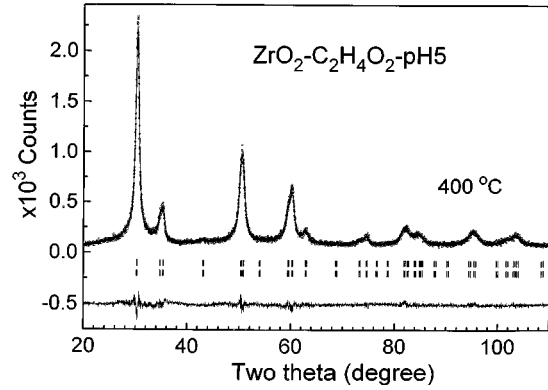


FIG. 8. Rietveld refinement plot of the sol-gel zirconia prepared with acetic acid and annealed in air at 400°C ($R_{wp} = 0.08$). Experimental data are indicated by dots, while the calculated curve obtained after the refinement is indicated with a continuous line. Upper and lower tick marks represent the tetragonal zirconia. R_F was 0.01 for each phase.

phase was also modeled with the local order of the monoclinic phase, but the fit was not as good as with the tetragonal local order.

Weight phase concentrations (Table 4) were obtained from the structure refinement. In the crystallization of the amorphous phase, both tetragonal and monoclinic zirconia nanophases coexisted (Tables 5 and 6), the tetragonal phase being the main phase. Here, the monoclinic nanophase had a smaller crystallite size than the tetragonal one. For both hydrochloric acid and acetic acid, this difference in crystallite size was present even after the samples were annealed at 600°C (Table 4). The observed monoclinic nanophase in the initial crystallization was not associated with any transformation of the tetragonal phase produced by the growing of the tetragonal crystallite size (12).

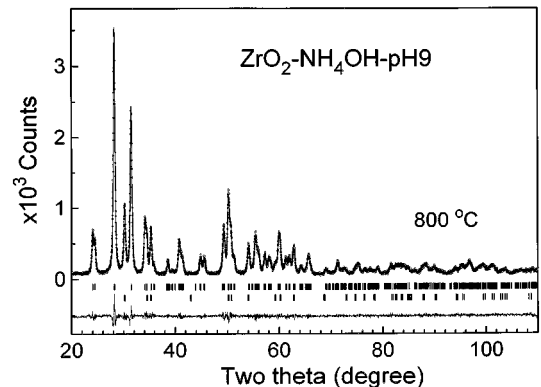


FIG. 9. Rietveld refinement plot of the sol-gel zirconia prepared with ammonium hydroxide and annealed in air at 800°C ($R_{wp} = 0.08$). Experimental data are indicated by dots, while the calculated curve obtained after the refinement is indicated with a continuous line. Upper tick marks represent the monoclinic phase ($R_F = 0.01$), and lower tick marks represent the tetragonal zirconia ($R_F = 0.01$).

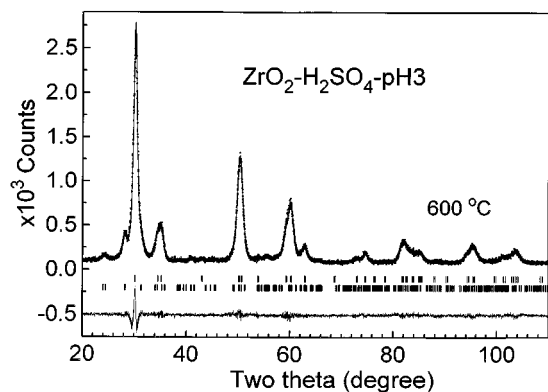


FIG. 10. Rietveld refinement plot of the sol-gel zirconia prepared with sulfuric acid and annealed in air at 600°C ($R_{wp} = 0.08$). Experimental data are indicated by dots, while the calculated curve obtained after the refinement is indicated with a continuous line. Upper tick marks represent the tetragonal phase ($R_f = 0.008$), and lower tick marks represent the monoclinic zirconia ($R_f = 0.01$).

To stabilize the tetragonal phase in microcrystalline zirconia at low temperatures, zirconia is doped with large ions such as Y, Ca, or Mg (5). In the sol-gel zirconia reported in the present work, however, the solutions and precursors used in the sample preparation did not include any of these or similar ions.

During sample preparation, H_2O , OH^- ions, H^+ ions, H_{ads} ions, and vacancies occur. When samples were annealed to 300°C, the H_2O present left them. Therefore, water did not stabilize the tetragonal structure. It is known that zirconia prepared from strongly acidic solutions ($pH < 1$) gives rise to the monoclinic phase (9, 28, 29), which also eliminated H^+ ions from stabilizing the tetragonal structure. Since the tetragonal structure that we observed was a bulk material, the adsorbed hydrogen was also discarded as the stabilizer. These results suggest that a mixture of OH^- ions and vacancies could cause the observed tetragonal structure stabilization.

From the Rietveld refinement of the tetragonal nanophase, we found that zirconium occupancy was less than 1.0. This corresponded to cation vacancies in the crystalline structure. For compensating electrical charge, these

TABLE 1
Tetragonal Zirconia (Space Group $P4_2/nmc$): Atomic Fractional Coordinates

Atom	Site	x	y	z
Zr	2a	0.75	0.25	0.75
O	4d	0.25	0.25	u

Note. u varied between 0.0467(9) and 0.050(2).

TABLE 2
Monoclinic Zirconia (Space Group $P2_1/c$): Atomic Fractional Coordinates

Atom	Site	x	y	z
Zr	4e	u_x	u_y	u_z
O(1)	4e	v_x	v_y	v_z
O(2)	4e	w_x	w_y	w_z

Note. These atomic fractional coordinates ranged within the limits specified in Table 3.

vacancies had to be close to OH^- ions occupying oxygen sites in the structure.

To detect and study OH^- ions in the zirconia structure, samples were analyzed by using FTIR spectroscopy.

FTIR spectra of fresh samples had absorption bands associated with residual water and solvent present after sample preparation. In all samples, these residues disappeared after sample annealing at 300°C.

When samples were annealed at higher temperatures, FTIR absorption bands associated with stable—even at 600°C—OH groups in the phase structures were observed.

For pH 3 and HCl as hydrolysis catalyst (Fig. 11a), the band produced by OH stretching vibrations was observed at 3318 cm^{-1} , while the band produced by its bending vibrations was observed at 1615 cm^{-1} . In the FTIR spectrum, bands produced by Zr-O binding were also detected. They were, however, not well defined, except the broad band at 381 cm^{-1} .

When the hydrolysis catalyst was sulfuric acid (pH 3), the bands produced by the stretching and bending vibrations of the stable OH groups shifted to 3417 and 1636 cm^{-1} , respectively (Fig. 11b), and had larger intensities than for the HCl hydrolysis catalyst. In the low-energy region of the spectrum, Zr-O binding produced well-defined bands at 606 and 459 cm^{-1} .

TABLE 3
Limits of the Fractional Coordinates of Monoclinic Zirconia

Fractional coordinate	Lower limit	Upper limit
u_x	0.2742(3)	0.2761(2)
u_y	0.0390(2)	0.0445(2)
u_z	0.2090(2)	0.2112(2)
v_x	0.064(1)	0.102(2)
v_y	0.329(1)	0.339(1)
v_z	0.328(1)	0.347(1)
w_x	0.425(1)	0.451(1)
w_y	0.756(1)	0.770(2)
w_z	0.430(2)	0.484(4)

TABLE 4
Zirconia Phase Composition and Average Crystallite Size as a Function of Hydrolysis Catalyst and Temperature

Hydrolysis catalyst	<i>T</i> (°C)	Tetragonal (wt%)	Monoclinic (wt%)	Tetragonal <i>d</i> (nm)	Monoclinic <i>d</i> (nm)
H ₂ SO ₄	600	85(3)	15(3)	12.4(4)	12(2)
	800	9(2)	91(4)	21.9(6)	27.8(8)
HCl	400	78(5)	22(4)	17(1)	4.1(2)
	600	35(1)	65(2)	24(1)	21(1)
	800	13(2)	87(3)	31(3)	31.1(8)
C ₂ H ₄ O ₂	400	62(3), 38(1)		12.5(6), 1.3(1)	
	600	91(1)	8.6(2)	22.0(5)	12.8(1)
	800	17(2)	82(3)	22(3)	29(1)
NH ₄ OH	400	70(5)	30(6)	8.4(3)	5.8(5)
	600	45(2)	55(1)	20.7(8)	22(1)
	800	11.7(4)	88.3(7)	32(3)	34(1)

TABLE 6
Zirconia Monoclinic Nanophase: Lattice Parameters as a Function of Hydrolysis Crystal and Temperature

Hydrolysis catalyst	<i>T</i> (°C)	<i>a</i> (nm)	<i>b</i> (nm)	<i>c</i> (nm)	β (deg)
H ₂ SO ₄	600	0.5135(5)	0.5198(5)	0.5321(4)	98.88(4)
	800	0.51417(4)	0.52030(4)	0.53127(4)	99.106(4)
HCl	400	0.5096(8)	0.5189(9)	0.5334(9)	98.1(1)
	600	0.51463(4)	0.51946(5)	0.53175(5)	99.07(3)
	800	0.51463(3)	0.51938(3)	0.53208(3)	99.163(3)
C ₂ H ₄ O ₂	400	0.494(2)	0.533(3)	0.556(2)	102.66(6)
	600	0.5146(5)	0.5197(5)	0.5313(5)	98.97(6)
	800	0.51463(4)	0.51973(4)	0.53165(4)	99.064(4)
NH ₄ OH	400	0.5158(5)	0.5192(5)	0.5305(5)	98.37(6)
	600	0.51436(5)	0.51986(5)	0.53147(5)	99.169(6)
	800	0.51433(2)	0.51981(3)	0.53170(3)	99.153(3)

For acetic acid as hydrolysis catalyst (pH 5), the band produced by OH stretching vibrations was shifted to 3381 cm⁻¹ and increased in intensity (Fig. 11c). The band associated with the corresponding bending vibrations, however, was not observed.

The shift of the band produced by the stretching vibration of the OH groups was stronger for ammonium hydroxide as hydrolysis catalyst (pH 9). This band was at 3417 cm⁻¹ in the FTIR spectrum (Fig. 11d), which suggested a stronger interaction between OH⁻ ions and the zirconia structure.

After the samples were annealed at 800°C, the observed FTIR bands associated with the OH groups had a very weak intensity.

TABLE 5
Zirconia Tetragonal Nanophase: Lattice Parameters as a Function of Hydrolysis Catalyst and Temperature

Hydrolysis catalyst	<i>T</i> (°C)	<i>a</i> (nm)	<i>c</i> (nm)
H ₂ SO ₄	600	0.35951(1)	0.51800(7)
	800	0.35945(5)	0.5182(2)
HCl	400	0.35975(5)	0.51749(4)
	600	0.35945(2)	0.51816(4)
	800	0.35945(2)	0.51839(7)
C ₂ H ₄ O ₂	400	0.35964(3)	0.51685(8)
	600	0.35941(1)	0.51804(3)
	800	0.35954(3)	0.51882(8)
NH ₄ OH	400	0.35989(5)	0.5165(2)
	600	0.35939(2)	0.51809(3)
	800	0.35953(3)	0.51877(8)

FTIR and X-ray diffraction results showed that the temperature behavior of the bands associated with the OH groups and the amount of tetragonal phase were correlated.

The foregoing analysis confirmed the presence of OH⁻ ions in sol-gel nondoped zirconia and reinforced the assumption that OH⁻ ions stabilized the tetragonal structure.

The assumption that OH⁻ ions and cation vacancies stabilized the tetragonal structure was according to the reported fact (30) that monoclinic zirconia is obtained when Zr(NO₃)₄ is used as a precursor in its preparation, but tetragonal zirconia is obtained when Zr(OH)₄ is the precursor.

The annealing of the samples at even higher temperatures increased the crystallite size of the nanophases and caused the transformation of the tetragonal nanophase into the monoclinic one (Figs. 3–6 and Table 4). According to our model of the stabilization of the tetragonal structure, when samples were annealed, the hydroxyl ions left them, destabilizing the tetragonal structure and transforming it into the monoclinic one. This transformation, however, was not reversible. Since the O²⁻ ions associated to the OH⁻ ions left the sample, the Ti:O molar ratio and the corresponding Ti–O bindings increased.

4. CONCLUSIONS

The structure of the zirconia produced by the sol-gel technique was amorphous when the samples were heated below 300°C. When sulfuric acid was the hydrolysis catalyst, however, the amorphous phase was stable at even higher temperatures. The local order in the amorphous structure was similar to the local order in the tetragonal phase.

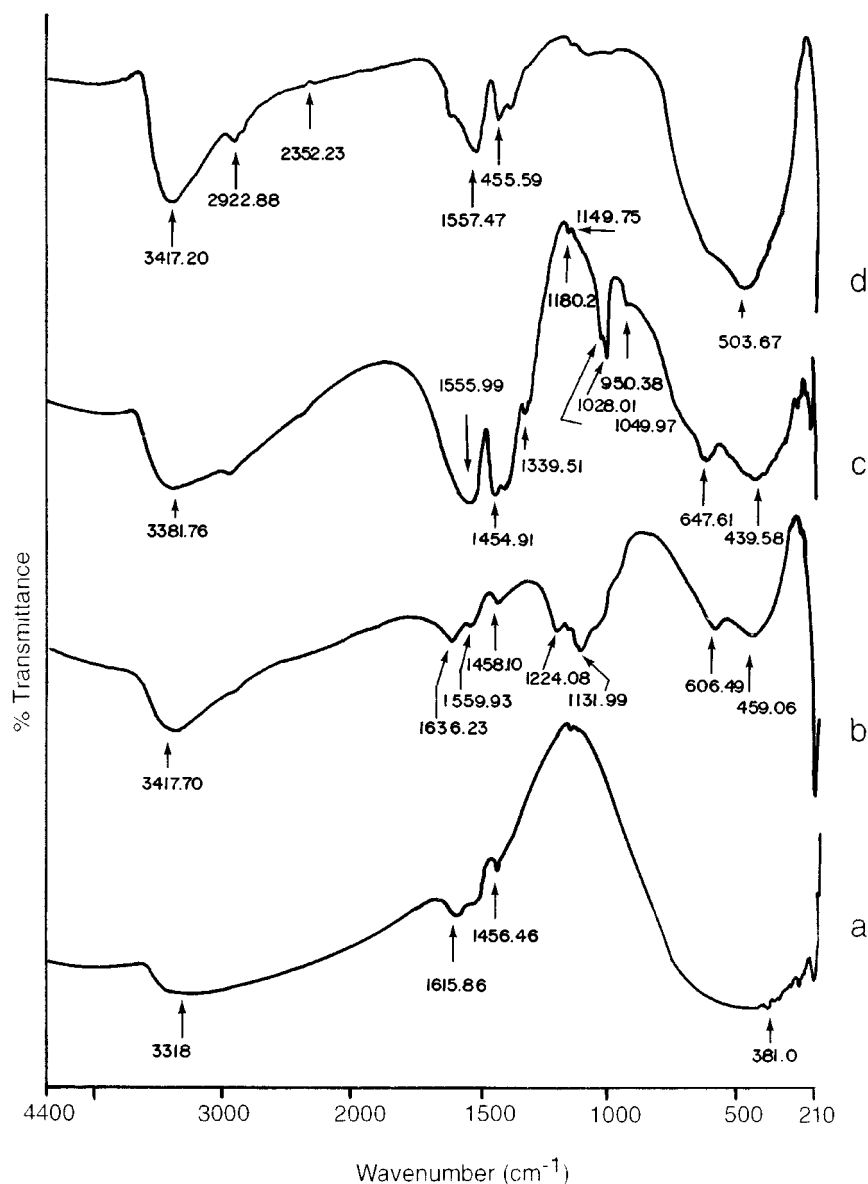


FIG. 11. FTIR transmittance curves of sol-gel zirconia annealed at 300°C and prepared with different hydrolysis catalysts: (a) hydrochloric acid, (b) sulfuric acid, (c) acetic acid, and (d) ammonium hydroxide.

For all hydrolysis catalysts, by annealing, the amorphous phase crystallized into the tetragonal and monoclinic zirconia nanophases, which coexisted since the beginning of crystallization. Here, the tetragonal phase was the main phase.

The average crystallite size of the monoclinic and tetragonal phases was similar. This result showed that the monoclinic nanophase can exist without needing to be generated by the transformation of the tetragonal phase when its crystal grows.

By annealing, the tetragonal phase was irreversibly transformed into the monoclinic phase. When acetic acid was the hydrolysis catalyst, the tetragonal zirconia nanophase was more stable.

We proposed a model for explaining the stabilization of the tetragonal phase. In this model, OH^- ions and Zr vacancies in the crystalline structure were the stabilizers. The model also explained the irreversible structure transformation of the tetragonal into the monoclinic phase, which was observed when samples were annealed.

REFERENCES

1. P. Reyer-Didier and H. Werke, *Ind. Ceram.* **839**, 449 (1989).
2. Q.-M. Yuan, J.-Q. Tan, and Z.-G. Jin, *J. Am. Ceram. Soc.* **69**, 265 (1986).

3. J. Fouletier, *Ceramurgia* **25**, 209 (1995).
4. Y. Ohno, Y. Kaga, and S. Nagata, *Electr. Eng. Jpn.* **107**, 59 (1987).
5. E. C. Subbarao, H. S. Maiti, and K. K. Srivastava, *Phys. Status Solidi* **21**, 9 (1974).
6. B. E. Yoldas, *J. Mater. Sci.* **21**, 1080 (1986).
7. G. Skandan, *Nanostruct. Mater.* **5**, 111 (1995).
8. K. T. Miller, C. J. Chan, M. G. Cain, and F. F. Lang, *J. Mater. Res.* **8**, 169 (1993).
9. R. P. Denkwicz, Jr., K. S. TenHuisen, and J. H. Adair, *J. Mater. Res.* **5**, 2698 (1990).
10. D. Michel, L. Mazerolles, P. Berthet, and E. Gaffet, *J. Solid State Inorg. Chem.* **32**, 673 (1995).
11. R. Gómez, T. López, G. Ferrat, J. M. Domínguez, and I. Schifter, *Chem. Lett.* 1941 (1992).
12. A. Chatterjee, S. K. Pradhan, A. Datta, M. De, and D. Chakravorty, *J. Mater. Res.* **9**, 253 (1994).
13. Y. Wang, K. Lu, D. Wang, Zh. Wu, and Zh. Fang, *J. Phys.: Condens. Matter* **6**, 633 (1994).
14. M. L. Rojas-Cervantes, R. M. Martín Aranda, A. J. López-Peinado, and J. de D. López-González, *J. Mater. Sci.* **29**, 3743 (1994).
15. R. Caruso, N. Pellegrini, O. De Sanctis, M. C. Caracoche, and P. C. Rivas, *Mater. Res. Soc. Symp.* **355**, 557 (1995).
16. A. Clearfield, *J. Mater. Res.* **5**, 161 (1990).
17. Zh. Lin and L. Zhang, *Rare Met. (Beijing)* **9**, 296 (1990).
18. P. F. Becher, *J. Am. Ceram. Soc.* **75**, 493 (1992).
19. Bokhimi, A. Morales, O. Novaro, T. López, E. Sánchez, and R. Gómez, *J. Mater. Res.* **10**, 2788 (1995).
20. R. A. Young, A. Sakthivel, T. S. Moss, and C. O. Paiva-Santos, *J. Appl. Crystallogr.* **28**, 366 (1995).
21. Margarita Schneider EDV-Vertrieb, Starnbergweg 18, D-8134, Pöcking, Germany, 1992, Tel. 0049-8157-8727, Fax 0049-8157-4527.
22. P. Thompson, D. E. Cox, and J. B. Hastings, *J. Appl. Crystallogr.* **20**, 79 (1987).
23. E. Prince, *J. Appl. Crystallogr.* **14**, 157 (1981).
24. A. Corma, V. Fornes, M. I. Juan-Rajadell, J. M. López-Nieto, *Appl. Catal. A* **116**, 151 (1994).
25. C. Monterra, G. Cerrato, C. Emanuel, and V. Bolis, *J. Catal.* **142**, 349 (1993).
26. F. C. Wu and S. C. Yu, *J. Mater. Sci.* **25**, 970 (1990).
27. A. Clearfield, G. P. D. Serrette, and A. H. Khazi-Syed, *Catal. Today* **20**, 295 (1994).
28. H. Saricimen, *Powder Technol.* **27**, 23 (1980).
29. P. E. D. Morgan, *J. Am. Ceram. Soc.* **67**, C-204 (1984).
30. R. Srinivasan and B. H. Davis, *Catal. Lett.* **14**, 165 (1992).